Eurographics Workshop on 3D Object Retrieval (2011)
H. Laga, T. Schreck, A. Ferreira, A. Godil, I. Pratikakis, and R. Veltkamp (Editors)

Real-Time 3D Face Recognition using Line Projection and Mesh Sampling

M.A. Rodrigues and A. Robinson

GMPR Geometric Modelling and Pattern Recognition Research Group
Sheffield Hallam University, Sheffield, UK

Abstract

The main contribution of this paper is to present a novel method for automatic 3D face recognition based on sampling a 3D mesh structure in the presence of noise. A structured light method using line projection is employed where a 3D face is reconstructed from a single 2D shot. The process from image acquisition to recognition is described with focus on its real-time operation. Recognition results are presented and it is demonstrated that it can perform recognition in just over one second per subject in continuous operation mode and thus, suitable for real time operation.

Categories and Subject Descriptors (according to ACM CCS): I.3.5 [Computer Graphics]: Computational Geometry and Object Modeling—Geometric algorithms, languages, and systems

1. Introduction

It is often stated that 3D facial recognition has potential advantages over 2D methods [Bowyer et al., 2004, Cook et al., 2006] as a number of limitations can be overcome including lighting variations and viewpoint dependency [Gordon, 1992, Medioni and Waupotitsch, 2003]. Moreover, 3D data can provide high accuracy on describing surface features such as cheeks and nose through curvature descriptors [Hesher et al., 2003]. This paper describes a real-time, fully automatic 3D face recognition system: from 2D eye tracking and image capture to 3D reconstruction, to 3D post-processing and recognition. It is noted that recognition is based on geometry alone: once an image is reconstructed in 3D, no texture information is used in the recognition process.

3D facial recognition algorithms based on geometry alone have been described with recognition rates up to 97% [Brink, 2008, Rodrigues et al., 2008] for selected models with low levels of noise. Furthermore, for special cases of high-density meshes with minimum noise accuracy of 100% are reported [Rodrigues and Robinson, 2009]. In those experiments, a person was enrolled once in the database from a standard frontal view and the verification models were reconstructed from different structured light images in which the person could be facing slightly left or right – is important to stress the carefully controlled environment and the role of relative noise free data in those experiments.

The availability of current 3D models and the format in which they are presented are not convenient for research aiming at fast recognition rates. While the Face Recognition Grand Challenge FRGC [FRGC, 2005] has allowed the wider research community to test recognition algorithms from standard 2D and 3D databases, a severe limitation is that it was not designed to cater for real-time requirements. The FRGC database is standardized such that an application can load pre-formatted data for feature extraction and recognition. 3D data were reconstructed from human subjects taken from a frontal, but arbitrary view point and, given that these are large files containing the structure of the vertices in 3D, this rules out the possibility of testing algorithms in a real-time scenario. Therefore, while FRGC 3D data are being profitably used to test recognition algorithms, the process does not represent a natural way in which 3D facial recognition systems are to be deployed.

Previous work from [Brink et al., 2008, Rodrigues et al., 2008, Rodrigues et al., 2007, Robinson et al., 2004, Robinson et al., 2004, Hall-Holt and Rusinkiewicz, 2001] have described structured light methods for fast 3D reconstruction from line projection. Commercial 3D face recognition using variations of structured light patterns are available such as

DOI: 10.2312/3DOR/3DOR11/009-016

from L1-Identity, Genex and ArtecID [Commercial 3D Face Recognition, 2011]. While these solutions differ substantially from the work presented here regarding capture device, pre- and post-processing operations and recognition methods, some conceptual similarities can no doubt be identified. These include 2D pre-processing, 3D post-processsing, feature extraction, enrollment and verification. A number of relevant aspects are discussed here. Section 2 describes 2D image processing and Section 3 the required 3D operations. Section 4 deals with pose normalization in 3D, Section 5 describes a sampling method, and Sections 6 and 7 present experimental results. Finally conclusions are presented in Section 8.

2. Automatic Face and Eye Tracking in 2D

Our scanner has three major components: a near-infrared (NIR) projector capable of projecting a pattern of sharp lines that remain in focus over a large distance up to 5m. Two CMOS cameras are used one operating in the visible and another in the NIR spectrum. A beam splitter is placed in front of the cameras such that both cameras see the same portion of the world. Face and eye tracking are performed in the visible spectrum and, when the image satisfies given constrains (see below) the NIR projector is switched on and the image is taken with the NIR camera. The NIR image contains the projected lines forming a pattern of stripes that are then processed to recover the 3D structure of the face.

The Intel Microcomputer Research Lab has developed a highly optimized computer vision library (openCV) that is fine-tuned for the underlying processor type [Bradski and Posarevsky, 2000]. The Viola-Jones object detection framework [Viola-Jones, 2001, Viola-Jones, 2004] is available in openCV with built-in routines for real-time face detection based on Haar-like features. A great advantage of these libraries is that it is possible to train and use a cascade of boosted classifiers for rapid object detection for any arbitrary object [Adolf, 2003, Seo, 2009].

Since eye detection is not built-into OpenCV 1.0 (it is now included in OpenCV 2.0), we trained boosted classifiers with examples of left and right eye and negative images. The general problem with such detection techniques is the number of false positives. For instance, on any image there could be various detected faces and some might not be real faces. The same problem happens with eye detection; the routines normally detect more eyes than there are in the scene. In order to solve this problem a number of constraints are defined: first, there should be only one face detected in the image and the face width must be larger than a certain threshold (300 pixels in our case); second, there should be only one left and only one right eye detected in the image, and these must be within the region of interest set by the face detection; third, the position of the face and eyes must not have moved more than a set threshold since last detection (10 pixels in our case) so to avoid inconsistent shots caused by rapid motion.

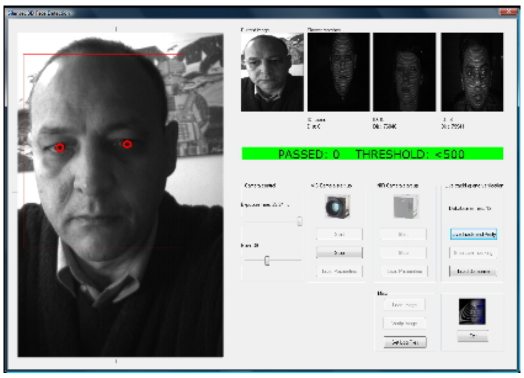

Figure 1: *Automatic face and eye tracking*

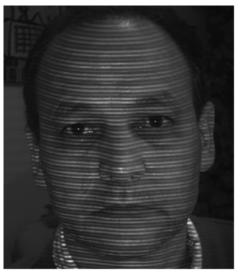

Figure 2: *Image with stripe patterns*

Figure 1 shows the system's interface; it is continuously tracking and detecting (possibly multiple) faces and eyes, but only when the above conditions are satisfied a shot is taken. In this way, the system is apparently idle until someone places their face in front of the camera. We have extensively tested face and eye detection and it works remarkably well in real-time. Before a shot is taken a near-infrared line pattern is projected onto the subject. The result is that we now have a structured light 2D image enabling 3D reconstruction and, from eye tracking, we know the position of the eyes in 2D from which we can know their 3D counterparts. The next step in the process is to apply 2D image filters such as median and weighted mean filters on the patterned image (Figure 2) followed by detection and indexing of the stripes. Given that we know the geometry of the camera and projector, by knowing the stripe indices we can now fully reconstruct in 3D by trigonometry. Details of the process have been published in [Robinson et al., 2004].

3. Automatic Pre- and Post-Processing in 3D

3D reconstruction is achieved by mapping the image space to system space (camera + projector) in a Cartesian coordinate system. We have developed a number of successful algorithms to deal with the mapping as described in [Brink et al., 2008, Robinson et al., 2004]. Once this mapping is achieved, a 3D point cloud is calculated and the output is triangulated using the connectivity of the vertices as depicted in Figure 3.

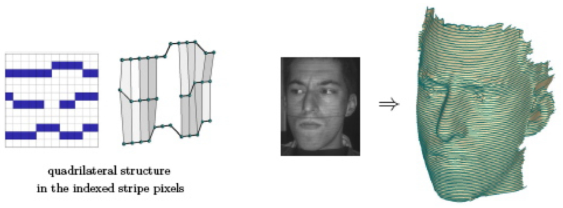

Figure 3: *Point cloud and triangulation from the detected stripe pattern in 2D*

Once the surface shape has been modeled as a polygonal mesh, a number of 3D post-processing operations are required: hole filling, mesh subdivision, smoothing, and noise removal. There are several techniques that can be used to fill in gaps in the mesh such as the ones discussed in [Tekumalla and Cohen, 2004, Wang and Oliveira, 2003, Wang and Oliveira, 2007]. From the techniques we considered, we tend to focus on three methods namely bilinear interpolation, Laplace, and polynomial interpolation. We found that the most efficient method for real-time operation is bilinear interpolation [Rodrigues and Robinson, 2009]. Mesh subdivision increases the mesh density and has the potential to render sampling more accurate. We use a polynomial interpolation of degree 4 across the stripe patterns resulting in more discernible features. This is demonstrated in Figure 4, where in the subdivided mesh (pink) the region around the eyes and lips are better delineated.

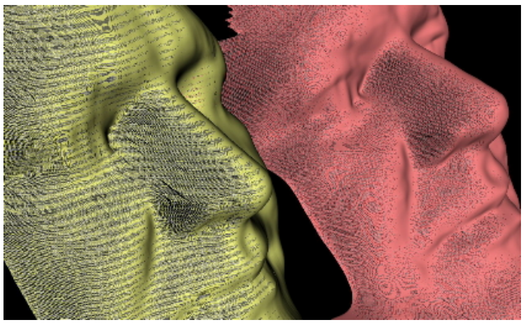

Figure 4: *Non-subdivided mesh (left) and subdivided (right)*

We tested two smoothing techniques namely moving average and Gaussian smoothing. Moving average is performed through cycling across and then along the stripes. The average of every three points is estimated and the middle point

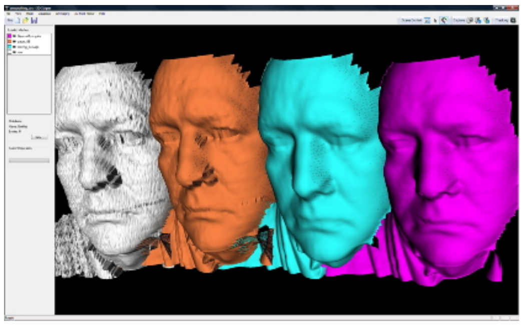

Figure 5: *The effects of smoothing from the left: the original model; Gaussian smoothing; moving average; Gaussian smooting followedd by moving average*

is replaced by the average. In this way the boundary vertices remain anchored. Gaussian smoothing is iteratively estimated by considering 8 neighbours for each vertex. A convolution mask of size 3×3 is applied and the centre vertex is perturbed depending on the values of its neighbours. The difference between each neighbour and the centre vertex is recorded and averaged as ΔV. A multiplier factor is provided (L) which determines how much of this average should be used to correct the value of the centre vertex; i.e., it defines the momentum of the error correction. We use $L = 0.9$ and the number of iterations is set to maximum 35. At each iteration cycle i, the centre vertex V is corrected by:

$$V_i = V_{i-1} + L\Delta V. \qquad (1)$$

A comparative analysis is depicted in Figure 5. It is clear that Gaussian smoothing (second model from the left) has considerable limitations regarding the perceived quality of the mesh. The moving average algorithm (third) seems to work considerably better. By running a Gaussian followed by a moving average slightly improves the model (fourth) especially around the lip area, which becomes more pronounced.

Noise removal is mainly concerned with the region around the eyes, as considerable amount of noise exist due to eyelashes and unwanted reflections. A natural solution is to replace vertices in the eye by a spherical surface. A sphere was centered at 40mm behind the face model in the same Z-axis as the centre of each eye. An elliptical mask is cut centred on each eye, and all vertices within the elliptical surface have their values replaced by their spherical counterparts. This however, resulted in unnatural looking models. A better solution, which is conceptually simpler, is to punch an elliptical hole centered at each eye and then fill in the holes with bilinear interpolation. This has proved to work well for the face models as shown in Figure 6. Finally, texture mapping can be overlaid on the mesh either by using the same striped image or by an identical image in the visible spectrum without stripe information. This is visualized in Figure 7, which

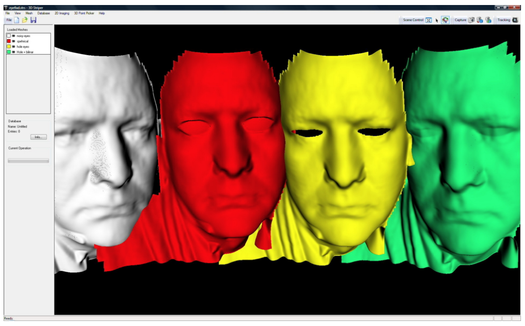

Figure 6: *Comparative analysis of noise removal around the eyes from left to right:original mesh; fitting an elliptical mask around the eyes and filling with a spherical surface centered at 40mm behind the model; punching an elliptical hole around the eyes; filling the elliptical hole with bilinear interpolation*

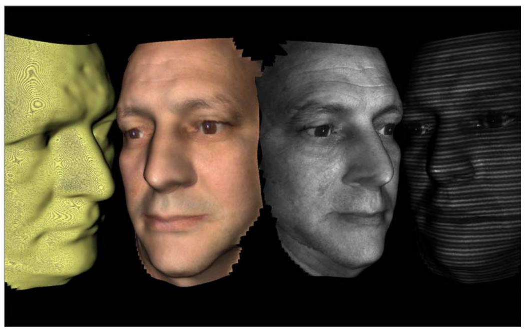

Figure 7: *Triangulated mesh (left), with color and black and white texture mapping (centre) and with original stripe pattern (right)*

shows from left to right the triangulated model, with color and black and white texture, and with the original projected stripe pattern. This is also useful for integrating 2D and 3D face recognition algorithms.

4. Pose Normalization

All models in the database need to be brought to a standard pose. The pose needs to be consistent, i.e., it should be possible to evaluate for all models. We have chosen the pose depicted in Figure 8 where the origin is placed at the tip of the nose. In this pose, the X-axis (red) is aligned with the position of the eyes, the Y-axis (yellow) forms a constant angle of $\pi/10$ with a point located on the front between the two eyes, and the Z-axis points away from the model such that all depths are negative. The algorithm to achieve this standard pose is described as follows (given that we know the position of the eyes (E_1 and E_2) in 3D:

1. Estimate the angle β_1 in the XY-plane between E_1 and E_2

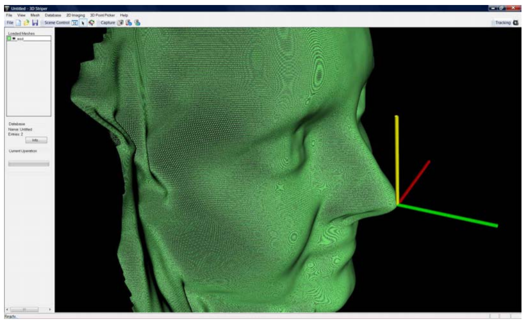

Figure 8: *The standard normalized pose with the origin at the tip of the nose*

2. Centered on E_1 rotate the mesh around the Z-axis by angle $\beta_1 : Rot(z,\beta_1)$
3. Estimate the angle β_2 in the YZ-plane between E_1 and E_2
4. Centered on E_1 rotate the mesh around the Y-axis by angle $\beta_2 : Rot(y,\beta_2)$
5. Find the intersection point F on the mesh (above the eyes, on the front) of the arcs centered on E_1 and E_2 with radius 0.75 of the inter-ocular distance
6. Find the tip of the nose T. This is defined as the highest point on the mesh below eye positions within a search threshold of one inter-ocular distance
7. Estimate the angle β_3 described by F, T, and the Y-axis
8. Centered on T, rotate the mesh around the X-axis by $(\pi/10-\beta_3) : Rot(x,\pi/10-\beta_3)$
9. After this rotation, the highest point on the mesh defining T might have slightly changed. Repeat steps 6, 7 and 8 until $(\pi/10-\beta_3)$ is below a set threshold.

5. Mesh Sampling

First, define a region on the face from which sampling points are to be taken. The region is cropped in 3D analogous to cropping a 2D image: we define two horizontal planes (top and bottom) and two vertical planes (left and right) setting the limits for cropping the 3D structure. All calculations are performed in 3D and if a point lies within the boundaries of the four cropping planes it is marked as valid, otherwise it is marked as invalid. The result is a cropped face structure, or a face mask from which a fixed number of points are sampled. We chose to sample 900 points (30×30). These points form the feature vector that uniquely characterizes a face and it is used for recognition. Figure 9 shows the original face structure in blue and the sampled mask in white.

The starting point from cropping and sampling is the position of the two eyes in 3D. This is known from 2D eye tracking, from which corresponding 3D vertices can be determined. The idea is to cut the mesh in 3D half a distance between the eyes to the left and right of each eye, and 1/3 of the distance to the top and 2/3 of the distance to the bottom.

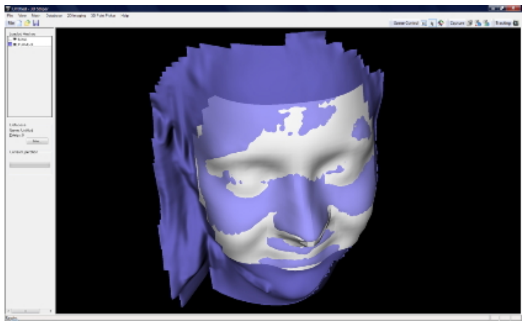

Figure 9: *Sampling method: a mask (light color) is cut from the model (darker). The mask contains 900 points whose depths are used for recognition*

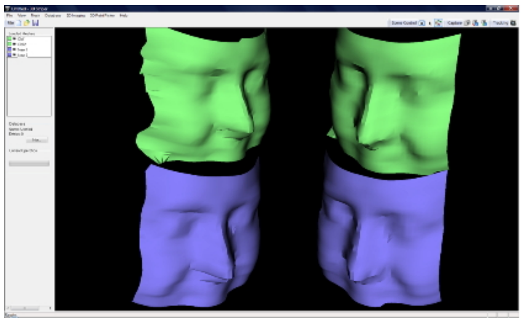

Figure 10: *Boundary noise in cropped face models. The noisy side of the geen model (top left) is corrected by point reflection, resulting in the blue model*

Recalling that the mesh has been normalized so the origin is at the tip of the nose and the reference distance is the inter-ocular distance $(E2-E1)$ where E_1 and E_2 are the locations of the two eyes in 3D. A rectangular sampling mask is defined through four cropping planes as follows.

- $\Pi_{\mathbf{TOP}}$: a plane parallel to XZ-plane defined at point $(0, 1.3(E_2-E_1), 0)$
- $\Pi_{\mathbf{BOTTOM}}$: a plane parallel to XZ-plane defined at point $(0, -0.66(E_2-E_1), 0)$
- $\Pi_{\mathbf{LEFT}}$: a plane parallel to YZ-plane defined at point $(-(E_2-E_1), 0, 0)$
- $\Pi_{\mathbf{RIGHT}}$: a plane parallel to YZ-plane defined at point $((E_2-E_1), 0, 0)$

Noisy regions at the boundaries of the cropped face present a serious problem as shown in Figure 10. The green models show both sides of the cropped face. When the shot was taken, the person was looking to their right, assuming a similar pose to the green model on the right. A clear view of that side of the face is available while the other side is partially occluded. Stripes are projected horizontally on the face and because some stripes stretch further than others, it is possible to fill in a number of holes in the occluded area, but this is never a perfect job, as it can be seen on the green model on the left.

The solution to this problem is to reflect the good points on one side of the mesh replacing the noisy ones on the other side. Only a few points are required to be reflected and the decision as to how many points and which side of the face needs to be reflected is made depending on whether the mesh has been rotated clockwise or anti-clockwise in the Y-axis (yellow axis in Figure 8) and by how much. For the sampling mask 30×30, these are the values for the number of reflected points N :

- If rotation angle $0.00 < abs(\beta_2) \leq 0.10, N = 3$
- If rotation angle $0.10 < abs(\beta_2) <= 0.15, N = 6$
- If rotation angle $0.15 < abs(\beta_2) <= 0.20, N = 7$
- If rotation angle $0.20 < abs(\beta_2), N = 8$

Finally, if $\beta_2 > 0$, reflect points from right to left of the YZ-plane, otherwise from left to right. The result of reflecting such points is shown in the blue model on the left of Figure 10: its initial state was the green model above. It clearly becomes a better-defined model.

Since the starting point for cropping the face in 3D is the position of the eyes, it is a natural question to ask to what precision eyes need to be detected. In Figure 10 the white mask was cropped from the eye locations as detected by eye tracking. A difference of 10 pixels in an image of size 1392×1040 was added to each eye location, effectively making the distance between the two eyes 20 pixels wider. A wider eye distance means a larger cropped face in 3D; this is shown in the blue model of Figure 11. However, note that the feature vector is constructed from the depth of the 900 sampled points, so the actual difference in depth between the white and blue cropped faces is negligible (<0.1%) and should not impair recognition as shown in the next section.

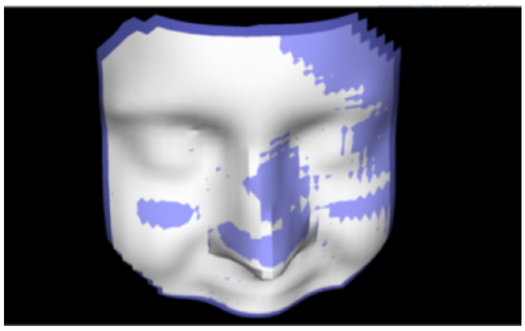

Figure 11: *Sensitivity to variations of 20 pixels in eye location*

6. Recognition Results

The eigenface method [Turk and Pentland, 1991] was used for recognition. Given that we wanted to test the feasibility

Table 1: *RECOGNITION RESULTS (CLOSEST MATCH)*

Sampling Mask Method		
Number of Entries in DB	Correctly Identified	Percentage
20	20/20	100
40	40/40	100
80	80/80	100
200	192/200	96

Table 2: *SAMPLE IDENTIFICATION (ONE-TO-MANY)*

Real Identity: p01		Real Identity: p02		Real Identity: p03	
Found in DB	Shortest distances	Found in DB	Shortest distances	Found in DB	Shortest distances
p01s2	43	p02s1	68	p03s2	19
p01s1	53	p02s2	72	p03s1	22
p01s3	69	p01s1	85	p05s1	92
p01s4	71	p01s3	88	p05s2	102
p02s2	108	p04s1	88	p03s3	111
p02s1	121	p01s2	93	p04s2	135
p05s2	139	p04s2	96	p04s1	138
p04s1	147	p01s4	106	p03s4	143
p04s2	155	p05s2	111	p02s1	146
p05s4	155	p05s4	112	p02s2	154

of the method for real time operation, we performed identification (one-to-many) and extracted statistics from the log file. Four databases were created with 20, 40, 80, and 200 entries. For enrollment, 2 models of each person were used: one frontal and another looking to the side (either right or left) as in the example shown in Figure 12.

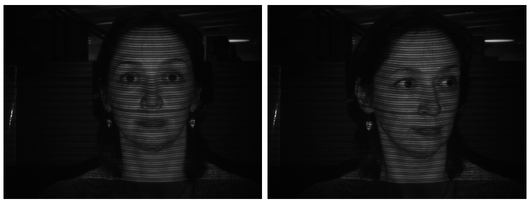

Figure 12: *Examples of enrolment shots*

For enrolment, if the identity of the person were person 01, the model in the database would be enrolled as p01s1, p01s2, p01s3, p01s4 (person 01 shot 1, person 01 shot2, person 01 shot 3, person 01 shot 4). It is important to stress that in the tests reported here we have not tried to select noise-free models: all models were selected at random so some models contain high levels of noise. Recognition results are summarized in Table 1 for the closest match in the database.

In performing identification (one-to-many) we saved to a spreadsheet the results of the 10 closest matches so we can reason about setting thresholds for verification. Obviously that for different sizes of databases the threshold varies and the correct threshold to minimize FAR can only be found by experimentation. As an example of determining the correct threshold for verification, Table 2 shows the sorted results for 3 subjects only where correct identification is colored green. It is clear that some models are more distinctive than others and over the database the top two results point to the right identity. A reasonable threshold for verification for this database would thus be a distance of 72. This is the worse case scenario meaning that for any person performing verification on this database if the distance to the claimed model is 72 or less it would be considered a pass.

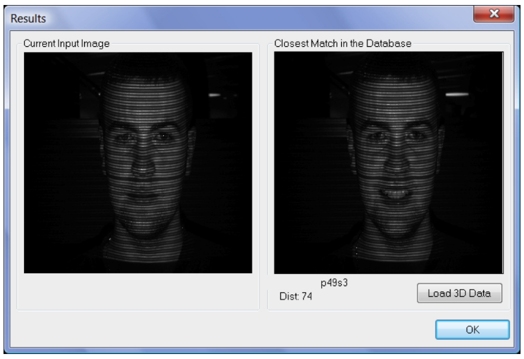

Results

Current Input Image

Closest Match in the Database

p49s3

Dist: 74

Figure 13: *An example of correct identification (one-to-many). Left input model; right, enrolled model*

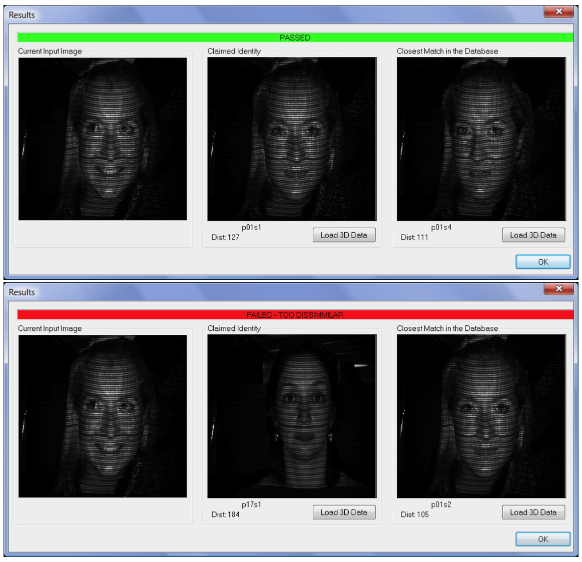

Results

PASSED

Current Input Image

Claimed Identity

p01s1

Dist: 127

Closest Match in the Database

p01s4

Dist: 111

Results

FAILED - TOO DISSIMILAR

Current Input Image

Claimed Identity

p17s1

Dist: 184

Closest Match in the Database

p01s2

Dist: 105

Figure 14: *Examples of passed (top) and failed verification (bottom)*

The sampling method is also shown to be robust to variations in expression as illustrated in Figure13, which shows a typical example of one-to-many identification. The input model (by definition unseen) has its closest match in person 49 shot 3, which is the correct model with a smiley face. The database has 200 entries and a measure of the distance (74) between input model and closest match is displayed.

Verification is depicted in Figure 14 where the model on the left is the input, the centre is the claimed identity (enrolled), and the right is the closest match in the database (we extended the verification procedure to also retrieve the closest match). The threshold for verification was set at 150, based on information from a table similar to the one depicted in Table 1. On the top image, the claim is accepted as the distance is smaller than the threshold and a green banner shows "PASSED". Note that the two enrolled models (centre and right) do not smile. On the bottom, the claim is not accepted as the distance is greater than the threshold and a red banner with the message "FAILED: TOO DISSIMILAR" is displayed. Note that this time the closest match in the database is not the same as above (given small differences in eye detection) but still the correct person.

Concerning the misclassifications in Table 1, the reasons for these are clear and have to do with camera calibration issues and noise in the eye region. It has been established that, on data collection, the camera focus was changed between enrollment and verification causing the scale of the models to change. Effectively, calibration is thrown out by a change of focus. In addition, noise in the eye region has resulted in inaccurate pose normalization. This is illustrated in Figure 15 in which the green model is the enrolled one and the wire mesh is the verification model. It is clear that a large number of points at the boundaries differ substantially and this resulted in a closest match to a different model in the database. The lessons from these misclassifications are twofold: first, it is necessary to run the subdivision algorithm, as subdivision tends to reduce noise around the eyes (all models were generated without subdivision). Second, if the camera focus is changed for whatever reason during data collection, the camera needs to be recalibrated before proceeding – this seems obvious and had we spotted these problems before enrolling and verifying, uncalibrated models would have been removed from the database and we would probably have gotten perfect recognition results for these tests.

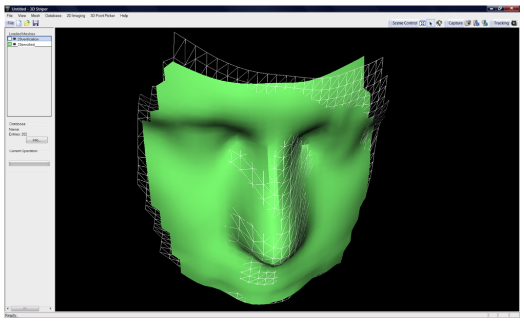

Figure 15: *A failed identification due to scale and noise*

7. Real Time Performance

The algorithms were tested working together from eye tracking to 3D reconstruction and recognition including logging the results with time stamps onto an HTML file. We used a Sony Vaio computer, Intel Core 2 Duo, 2.4GHz, 4GB memory. It has been shown that the methods presented here lend themselves to real-time operation as, from the moment the eye tracking algorithms lock on the eyes, it takes only 1second 200millisencods to perform the following operations:

- Take a shot in 2D
- Run 2D image filters
- Detect the stripes in the image
- Convert the stripes into a 3D point cloud
- Triangulate the point cloud
- Perform hole filling on the mesh
- Determine the location of eyes in 3D
- Punch a hole in the eyes, fill in with bilinear interpolation
- Find tip of the nose
- Normalize pose with origin at the tip of the nose
- Determine the cropping planes and crop the mesh
- Replace noisy points by reflection
- Sample the cropped mesh to 900 points
- Search the database for the closest match
- Display results of recognition on screen
- Save to log file: time stamp, current image, closest match
- Continue eye tracking and repeat the sequence

This is indeed a remarkable performance given the size of the mesh (>20,000 data points per face model), the high number of operations and the complexity of the required functions. Thread functions were implemented where required for improved performance and there is scope for further optimization by expanding thread granularity. In a recent trial at Heathrow Airport (London, UK) the requirements were set at maximum 10seconds per subject for 3D face recognition. Our solution is one order of magnitude better than those requirements and thus, can be realistically applied where high throughput 3D face recognition is required.

8. Conclusion

This paper has presented methods for real-time 3D face recognition from face and eye tracking in 2D to fast 3D reconstruction, to feature extraction by mesh sampling, to identification and verification. Based on geometry alone, the reported recognition accuracy is excellent and there is the potential to achieve 100% recognition for small databases (200 enrolled models were tested). The misclassified cases were traced back to camera calibration issues.

It is important to stress that the objective of the paper was not to compare the recognition method based on sampling the mesh with other recognition methods reported in the literature that use FRGC data. We argued in the introduction that FRGC data are not suitable for real-time operation because video stream data with face and eye tracking are required to demonstrate real-time capabilities by generating 3D data on the fly. We thus use our own purpose built 3D scanner in conjunction with our own fast 3D reconstruction algorithms. We have demonstrated in this paper that the process from 2D tracking to 3D recognition takes only just one second per subject and thus, can be used in a real-time scenario.

Future work includes testing the limits of recognition for a large databases, and designing and implementing a method for fully automatic camera calibration. We are also pursuing research on mesh description using partial differential equations (PDEs) and developing recognition methods that use PDE information. Furthermore, methods to compress the 3D mesh are required to enable network-based 3D recognition systems. Research on these issues is under way and will be reported in the near future.

References

[Adolf, 2003] ADOLF, F.: How to build a cascade of boosted classifiers based on Haar-like features. http://lab.cntl.kyutech.ac.jp/kobalab/nishida/opencv/OpenCObjectDetectionHowTo.pdf

[Bowyer et al., 2004] BOWYER, K.W., CHANG K., AND FLYNN P.: A Survey Of Approaches To Three-Dimensional Face Recognition, *Int Conf on Pattern Recognition* , (ICPR 2004) 358-361.

[Bradski and Posarevsky, 2000] BRADSKI, G.R AND V. PISAREVSKY: Intel Computer Vision Library: applications in calibration, stereo segmentation, tracking, gesture, face and object recognition. *Proceedings IEEE Conference on Computer Vision and Pattern Recognition* (2000) vol. 2, 796-797.

[Brink, 2008] BRINK,W.: 3D Face Scanning and Alignment for Biometric Systems, *PhD Thesis*, Sheffield Hallam University, 2008.

[Brink et al., 2008] BRINK, W., A. ROBINSON, M. RODRIGUES: Indexing Uncoded Stripe Patterns in Structured Light Systems by Maximum Spanning Trees, *British Machine Vision Conference* (BMVC 2008) Leeds, UK, 1-4.

[Commercial 3D Face Recognition, 2011] COMMERCIAL 3D FACE RECOGNITION SYSTEMS: L1-IDENTITY, GENEX, ARTEC. http://www.l1id.com/, http://www.genextech.com/, http://http://www.artecid.com/

[Cook et al., 2006] COOK, J., C. MCCOOL, V. CHANDRAN, AND S. SRIDHARAN: Combined 2D/3D Face Recognition Using Log-Gabor Templates, Advanced Video and Signal Based Surveillance, *IEEE Intl Conf on Advanced Video and Signal Based Surveillance* (AVSS 2006) pp. 83.

[FRGC, 2005] FRGC: The Face Recognition Grand Challenge, http://www.frvt.org/FRGC/

[GMPR, 2009] GMPR: Geometric Modelling and Pattern Recognition Video Demos. http://www.shu.ac.uk/research/meri/gmpr/videos.html

[Gordon, 1992] GORDON, G.: Face recognition based on depth and curvature features. *Computer Vision and Pattern Recognition* (CVPR 1992) 108-110.

[Hall-Holt and Rusinkiewicz, 2001] HALL-HOLT, O. AND RUSINKIEWICZ, S.: Stripe Boundary Codes for Real-Time Structured-Light Range Scanning of Moving Objects. (ICCV 2001), pp. 359-366.

[Hesher et al., 2003] HESHER, C., A. SRIVASTAVA, AND G. ERLEBACHER: A novel technique for face recognition using range images. *Proc 7th Int Symposium on Signal Processing and Its Applications* (ISSPA 2003) Paris.

[Medioni and Waupotitsch, 2003] MEDIONI, G. AND R.WAUPOTITSCH: Face recognition and modeling in 3D. *IEEE International Workshop on Analysis and Modeling of Faces and Gestures* (AMFG 2003), 232-233.

[Rodrigues and Robinson, 2009] RODRIGUES, M.A, AND A. ROBINSON" Novel Methods for Real-Time 3D Facial Recognition. In *Strategic Advantage of Computing Information Systems in Enterprise Management: Part V: Computer Modelling.* Majid Sarrafzadeh and Panagiotis Petratos (eds.) pp, 169-180, ISBN: 978-960-6672-93-4, ATINER, Athens, Greece, 2010.

[Rodrigues et al., 2008] RODRIGUES, M.A., A. ROBINSON, AND W. BRINK: Fast 3D Reconstruction and Recognition. In *New Aspects of Signal Processing, Computational Geometry and Artificial Vision* ISCGAV 2008, Rhodes, pp. 15-21.

[Rodrigues et al., 2007] RODRIGUES, M.A., A. ROBINSON, AND W. BRINK: Issues in Fast 3D Reconstruction from Video Sequences. *Lecture Notes in Signal Science, Internet and Education, Proceedings of 7th WSEAS International Conference on MULTIMEDIA, INTERNET and VIDEO TECHNOLOGIES* (MIV 2007), Beijing, China, (Sep 2007) 213-218.

[Rodrigues et al., 2006] RODRIGUES, M.A., A. ROBINSON, L. ALBOUL, AND W. BRINK: 3D Modelling and Recognition. *WSEAS Transactions on Information Science and Applications* Issue 11, Vol 3, 2006, 2118-2122.

[Robinson et al., 2004] ROBINSON, A., L. ALBOUL, AND M. RODRIGUES: Methods for indexing stripes in uncoded structured light scanning systems. *Journal of WSCG* 12(3) 371-378, 2004.

[Robinson et al., 2004] ROBINSON, A., M.A. RODRIGUES, AND L. ALBOUL: Producing Animations from 3D Face Scans. *Game-On 2005 6th Annual European GAME-ON Conference* De Montfort University, Leicester, UK, Nov 23-25, 2005.

[Seo, 2009] SEO, N.: *Tutorial: OpenCV haartraining (Rapid Object Detection With A Cascade of Boosted Classifiers Based on Haar-like Features)* http://note.sonots.com/SciSoftware/haartraining.html

[Tekumalla and Cohen, 2004] TEKUMALLA, L.S., AND E. COHEN: A hole filling algorithm for triangular meshes. *Tech. Rep. University of Utah* December 2004.

[Viola-Jones, 2004] VIOLA, P. AND JONES, M.: Robust Real-Time Face Detection. *IJCV* 57(2):137-154 (2004)

[Viola-Jones, 2001] VIOLA, P. AND JONES, M.: Rapid Object Detection using a Boosted Cascade of Simple Features. *CVPR* (1) 2001:51-518, 2001.

[Wang and Oliveira, 2003] WANG, J. AND M. M. OLIVEIRA: A hole filling strategy for reconstruction of smooth surfaces in range images. *XVI Brazilian Symposium on Computer Graphics and Image Processing* (Oct 2003) pp 11-18.

[Wang and Oliveira, 2007] WANG, J. AND M. M. OLIVEIRA: Filling holes on locally smooth surfaces reconstructed from point clouds. *Image and Vision Computing* 25(1):103-113, January 2007.

[Turk and Pentland, 1991] TURK, M.A. AND A. P. PENTLAND: Face Recognition Uisng Eigenfaces. *Journal of Cognitive Neuroscience* 3 (1): 71-86.